Eur. Phys. J. Spec. Top.
https://doi.org/10.1140/epjs/s11734-025-01867-7

THE EUROPEAN PHYSICAL JOURNAL SPECIAL TOPICS

Regular Article

# Isochronous islands in the two-harmonic standard map

Michele Mugnaine[1,5,a], Bruno B. Leal[1,6,b], Alfredo M. Ozorio de Almeida[2,c], Ricardo L. Viana[3,4,d], and Iberê L. Caldas[1,e]

[1] Institute of Physics, University of São Paulo, São Paulo 05508090, Brazil
[2] Brazilian Center for Research in Physics, Rio de Janeiro 22290-180, Brazil
[3] Department of Physics, Federal University of Paraná, Curitiba 82590-300, Paraná, Brazil
[4] Interdisciplinary Center for Science, Technology, and Innovation, Curitiba 81530-000, Paraná, Brazil
[5] Lorena School of Engineering, University of São Paulo, Lorena 12602-810, São Paulo, Brazil
[6] Aix-Marseille Université, Marseille, France

Received 30 April 2025 / Accepted 17 August 2025


**Abstract** Isochronous islands are regular solutions related to different chains of elliptic points but with the same winding number. These isochronous islands emerge in phase space as a response to multiple resonant perturbations and can be simulated using a simple discrete model called the two-harmonic standard map. We observed three types of isochronous transitions, which can be formed through saddle-node and pitchfork bifurcations.

## 1 Introduction

In dynamical systems, isochronous islands are distinct regular solutions with the same frequency(rotation number) that surround different elliptic points of the same period. In the plasma physics literature, such islands are called heteroclinic and recent studies present theoretical and experimental evidence of the emergence of such islands within magnetically confined plasmas in tokamaks [1, 2]. In the plasma, for example, isochronous islands occur due to the interaction between multiple tearing modes which grow in the same rational surface, which lead to heteroclinic/isochronous bifurcations responsible for the emergence of the islands [1]. The presence of isochronous islands are identified in several dynamical models related to nonlinear oscillators [3], electron beam interactions with electrostatic waves[4], periodic lattices[5], molecular physics [6], billiards [7] and, as already mentioned, plasma physics [1, 2, 8, 9].

These isochronous bifurcations can be simulated by a simple discrete model, named the two-harmonic standard map (THSM), proposed and analyzed in Ref. [10] as a model for the competition between different resonant modes. According to the Poincaré–Birkhoff theorem, any resonance with a rational winding number $r/s$ leads to the emergence of $2k$ periodic orbits with period $s$, with $k \in \mathbb{N}$,[11] which moves $r$ steps in the positive direction [12]. In this scenario, half of these orbits are unstable (hyperbolic points) and the other half is stable. If $k > 1$, we have distinct islands with the same winding number, i.e., isochronous islands.

It was shown that isochronous islands emerge in the phase space as a response to multiple resonant perturbations and the number of islands depends on the system's characteristic and the amplitude perturbations. The isochronous islands occurs in the same winding number surfaces, i.e., only modes with the same ratio as winding number can interact and cause the emergence of isochronous islands. The winding number $(r_1, s_1)$ can be different than $(r_2, s_2)$, but the ratios $r_1/s_1$ and $r_2/s_2$ must be equal [8]. Besides the THSM, more complex models can also present

B. B. Leal, A. M. O. de Almeida, R. L. Viana, I. L. Caldas: These authors contributed equally to this work.

[a] e-mail: mmugnaine@gmail.com (corresponding author)
[b] e-mail: bruno.borges.leal@alumni.usp.br
[c] e-mail: alfredozorio@gmail.com
[d] e-mail: rlv640@gmail.com
[e] e-mail: ibere@if.usp.br

Published online: 26 August 2025

the emergence of isochronous islands[4, 8]. As shown for the THSM, sadlle-node and pitchfork bifurcations formed the transitions responsible for the emergence of isochronous islands in the same frequency surface [10].

In this paper, we consider and discuss isochronous bifurcations for other modes not presented in Ref. [10]. In Sect. 2, we present the two-harmonic standard map model and discuss the role of each competing model in the system. The competition between the modes and the isochronous transitions are analyzed in Sect. 3. Our conclusions are presented in Sect. 4.

## 2 The model

The two-harmonic standard map is proposed as a generalization of the extended standard map, investigated in Refs. [13–20], and it is defined by the equations[10]:

$$\begin{aligned} x_{n+1} &= x_n + y_{n+1}, \\ y_{n+1} &= y_n - \frac{K_1}{2\pi m_1}\sin(2\pi m_1 x_n) - \frac{K_2}{2\pi m_2}\sin(2\pi m_2 x_n), \end{aligned} \tag{1}$$

where $K_1$, $K_2 \in \mathbb{R}$ and $m_1$, $m_2 \in \mathbb{N}$. The two-harmonic standard map is a generic model to describe a dynamical system under the influence of two perturbations. A relationship between the perturbations produces a resonance-competing mode on the same KAM torus, leading to isochronous islands in phase space. The numbers $m_1$ and $m_2$ identify the wavenumbers of the perturbations and are referred to as the modes acting on the system. Each perturbation has an amplitude $K_i$, with $i = 1, 2$, and, depending on the values of the amplitudes, the system can exhibit $m_1$ to $m_2$ islands, with $m_2 > m_1$. We take mod 1 for both variables in (1).

To understand the effect of each mode, represented by each sine function in (1), we study each mode separately by computing the phase spaces for the system with only one non-zero perturbation. First, we consider $m_1 = 1$, $K_1 \neq 0$ and $K_2 = 0$. The resulting phase space is presented in Fig. 1a. As a second example, we choose $m_2 = 5$, $K_2 \neq 0$ and $K_1 = 0$, and, the phase space for this scenario is presented in Fig. 1b.

In Fig. 1a, we present the phase space for $m_1 = 1$, $K_1 = 0.01$ and $K_2 = 0$, i.e., we have just the perturbation related to mode $m_1$. For this scenario, we observe islands, indicated in blue, around the only elliptic orbit in line $y = 0$. The elliptic point has period 1 and it is centered in $(x, y) = (0, 0)$. For Fig. 1b, we present the phase space when the only mode in the system is $m_2 = 5$. The perturbation amplitudes are $K_1 = 0$ e $K_1 = 0.01$. In this case,

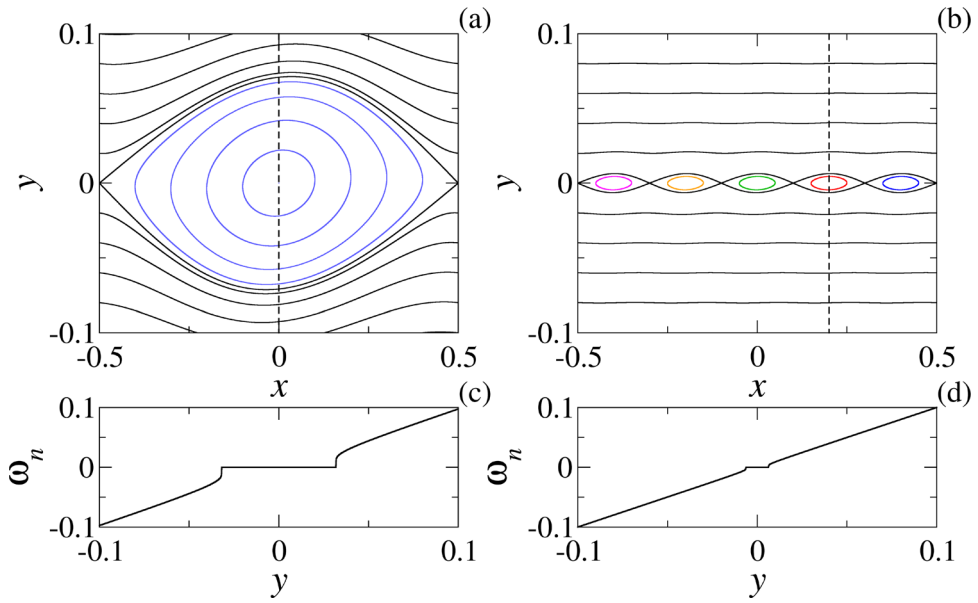


**Fig. 1** Phase spaces and winding number profile for isolated modes. In (**a**), we observe the phase space for $m_1 = 1$, $K_1 = 0.01$ and $K_2 = 0.0$. For (**b**), we have the isolated mode $m_2 = 5$, with $K_1 = 0$ e $K_2 = 0.01$. The winding number, defined in Eq. (2), is computed for each initial condition in the dashed lines indicated in the phase spaces. The respective winding number profiles for (**a**) and (**b**) are shown in panel (**c**) and (**d**). In phase spaces presented in (**a**) and (**b**), each color indicates a different isochronous island, i.e., regular solutions around different elliptic orbits

we observe five distinct islands circulating five distinct elliptic points of period 1 in $y = 0$. Each island is indicated by a different color to highlight that they are distinct solutions. These islands are called isochronous, they have the same period but are distinct islands.

We observe a similar structure in both phase spaces shown in Fig. 1. Each phase space is composed of quasi-periodic KAM-type curves, indicated by the black spanning curves, and islands surrounding elliptic points, indicated by the colored closed curves. The islands correspond to regular solutions around stable periodic orbits, *i.e.,* the fixed elliptic points of period 1.

With the phase spaces in Fig. 1a, b, we identify the effect of each mode in the system: the mode $m_{1,2}$ indicates the number of elliptic points of period 1 in $y = 0$. Along with the phase space, we also compute the winding number profile. The winding number is defined by the limit

$$\omega_n = \lim_{n\to\infty} \frac{x_n - x_0}{n}, \tag{2}$$

where the variable $x_n$ is lifted to the real line. If the limit in Eq. (2) converges, we have a regular orbit, which can be periodic or quasi-periodic. If the solution is chaotic, the limit does not converge. To compute the winding number in relation to $y$, we select $10^4$ initial conditions in the $x$ lines depicted in Fig. 1a, b as dashed lines, *i.e,* $x = 0$ for panel (a) and $x = 0.1$ for panel (b). We evolve each initial condition for $10^5$ iterations, compute the difference $x_n - x_0$ for each iteration and verify if it converges. The winding number profiles computed in the dashed lines of Fig. 1a, b are shown in Fig. 1c, d, respectively.

From the winding number profiles shown in Fig. 1c, d, we observe a monotonic increasing profile with a plateau centered in $y = 0$. The region of the profile where we observe an increasing relationship between the rotation number and $y$ corresponds to the invariant curves (black curves), since the rotation number of these curves depends on their position (*i.e.*, the value of $y$). In contrast, the plateau regions indicate the presence of islands, and their width reflects the extent of the island region, as the rotation number is constant for all islands surrounding a given elliptic point. The winding number value $\omega_n = 0$ is constant for the only island in Fig. 1a and for the five distinct islands in Fig. 1b. With this, we say the islands of both phase spaces are in the same winding number surface. As shown in Refs. [8–10], it is necessary for islands with the same winding number to lie on the same rational surface for isochronous bifurcations to occur. As discussed in more details in Ref. [10], when $K_1$ and $K_2$ are nonzero, we can have isochronous bifurcations, leading to transitions from mode $m_1$ to mode $m_2$. Now, we investigate the scenario with two modes acting on the systems, for nonzero $K_1$ and $K_2$.

## 3 Isochronous transitions

A $m_1 \to m_2$ transition occurs by isochronous bifurcations, i.e., the emergence of elliptic orbits on the same winding number surface, leading to the emergence of islands with equal winding number and isochronous behavior in the system. With this in mind, we investigate the bifurcation diagrams for the fixed points in the phase space. Setting $K_1 = 0.05$, we find the fixed points of the systems for increasing values of $K_2$. The fixed points are computed numerically by checking whether the orbit generated by a given point returns to its initial position. After that, we identify the stability via orbit convergence: if nearby orbits remain close (or diverge), the point is elliptic (or hyperbolic). We compute the bifurcation diagrams and phase spaces for the stages before and after the isochronous bifurcations.

We initiate our analysis by the case of Fig. 1, $m_1 = 1$ and $m_2 = 5$. The respective results are shown in Fig. 2.

In Fig. 2a, we have the bifurcation diagram for the fixed points of the case $m_1 = 1$ and $m_2 = 5$, with $K_1 = 0.05$. Up to $K_2 = 0.2$, we observe only one elliptic point and one hyperbolic points, the black and gray points at $x^* = 0$ and $x^* = 0.5$, respectively. At $K_2 = 0.2$, we observe the emergence of four pairs of black–gray points in the system. If we analyze the eigenvalues of the new fixed points, we observe that the black points have complex eigenvalues, *i.e.,*, elliptic points, while the gray points have real eigenvalues, indicating hyperbolic points. At the bifurcation point, the eigenvalues have modulus 1 (see Appendix for more information). The creation of a pair of elliptic–hyperbolic points is the consequence of saddle-node bifurcations. Here, we have four supercritical bifurcations, since we have the creation of fixed points [21, 22]. All four bifurcations occur at the same value of $K_2$, leading to a transition with no intermediate modes.

The phase space for the system before the transition is shown in Fig. 2b, for $K_2 = 0.04$. We observe only one island centered in the orange fixed point (0, 0). After the $1 \to 5$ transition occurred, we have the scenario depicted in Fig. 2c, where we observe five isochronous islands centered in elliptic points on line $y = 0$. The elliptic points are indicated by the colored points. As show in the diagram, all fixed points emerge by saddle-node bifurcations, characterizing the first observed type of transition from mode $m_1$ to $m_2$.

Next, we analyze the case where $m_1 = 3$ and $m_2 = 4$. From the bifurcation diagram, shown in Fig. 3a, we observe that there are only three elliptic points for $K_2 < 0.5$, indicating the predominance of mode $m_1 = 3$. For

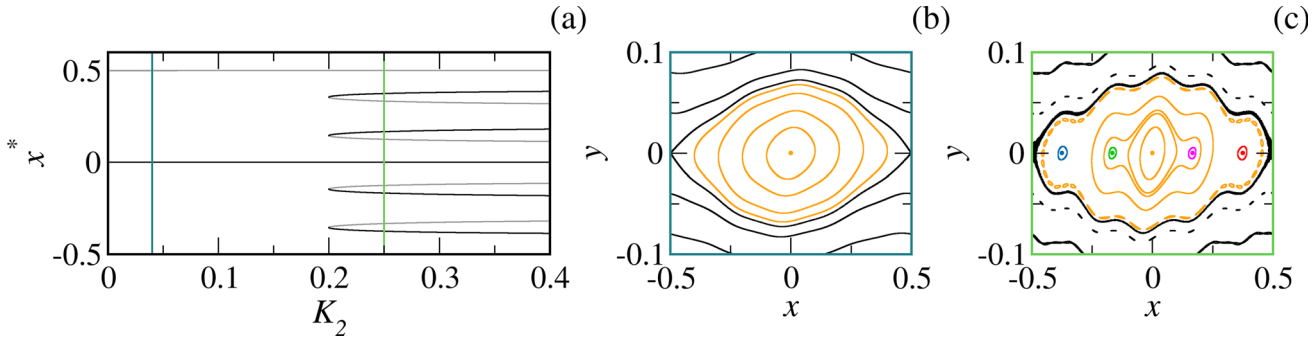


**Fig. 2** Transition from mode $m_1 = 1$ to $m_2 = 5$, with $K_1 = 0.05$. (**a**) The bifurcation diagram shows the evolution of the fixed points, where the elliptic and hyperbolic points are represented by black and gray points, respectively. We chose $K_2 = 0.04$ for the scenario before the isochronous bifurcations and $K_2 = 0.25$, for the scenario after it. Both values are highlighted by color vertical lines in panel (**a**). The respective phase spaces are shown in panels (**b**) and (**c**), where the frame color is related to the color line in (**a**). In the phase spaces, we use different colors to plot the islands surrounding distinct elliptic orbits. The invariant curves are shown in black and the colored points are the elliptic points

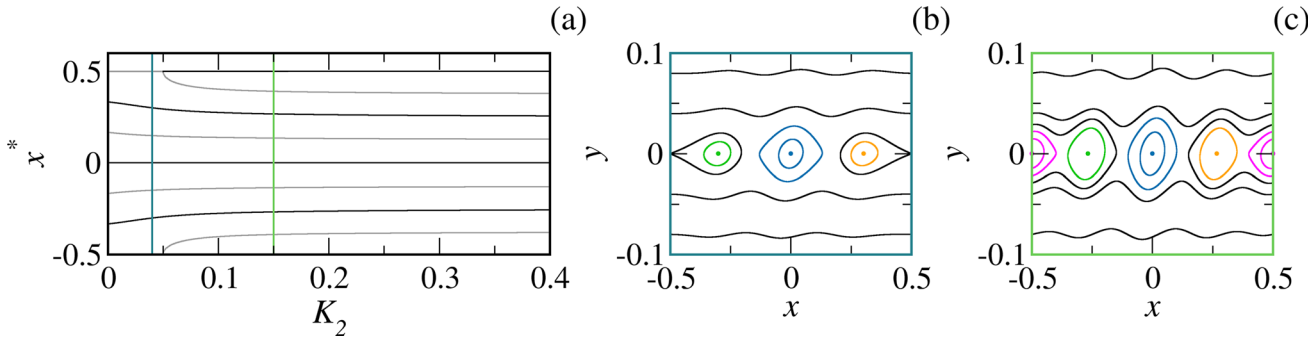


**Fig. 3** $3 \to 4$ transition by pitchfork bifurcation. In the bifurcation diagram in panel (**a**), we observe the occurrence of a pitchfork bifurcation at $K_2 = K_1 = 0.05$, where the hyperbolic point at $x^* = 0.5$ becomes elliptic and two new hyperbolic points emerge. The scenario before the transition is shown in (**b**), with $K_2 = 0.04$, while the scenario after the transition is depicted in (**c**), with $K_2 = 0.15$. As in Fig. 2, the black (gray) points in the bifurcation diagram indicate stable (unstable) fixed points. For the phase spaces, each color represents the islands that surround different elliptic points indicated by the same color

higher values of $K_2$, we have the emergence of one new elliptic point in $x^* = 0.5$ and the total of elliptic points on the line $y = 0$ is four. The new elliptic point emerges in a different manner compared to the scenario observed in the bifurcation diagram of Fig. 2. In this case, the hyperbolic fixed point at (0.5, 0) (gray point) becomes elliptic (black point) at the bifurcation, and two new hyperbolic points emerge on either side of it. Here, we observe the occurrence of a pitchfork bifurcation. This kind of bifurcation occurs in systems which have symmetry, for example, if a systems satisfies $f(-x) = -f(x)$ [22, 23]. The standard map and the two-harmonic standard both satisfy this relation for $x$ and $y$, thus they are symmetric with respect to the symmetry $x \to -x$ and $y \to -y$, which makes the pitchfork a possible bifurcation in the system.

From the bifurcation diagram shown in Fig. 3a, we observe that the $3 \to 4$ transition occurs by a pitchfork bifurcation in the hyperbolic point at $x^* = 0.5$. In the bifurcation, the hyperbolic point becomes elliptic and two new hyperbolic points emerge in the system. Before this isochronous transition, we have the scenario depicted in Fig. 3b, where we observe three islands identified with different color. The hyperbolic point at $x = 0.5$ is highlighted by the presence of a separatrix structure. A post-transition scenario is shown in Fig. 3c, a phase space with four islands. We observe that the "separatrix" structure disappears and a new island, centered at $x = 0.5$, emerges in the phase space. The sequence of Fig. 3 represents the second type of possible transition, that is, a transition by pitchfork bifurcation with no intermediate mode. We present a eigenvalue analysis fro the pitchfork bifurcation in the Appendix.

Finally, we investigate the $2 \to 5$ transition, which represent the third type of transition characterized by the presence of intermediate modes, *i.e.,* an island structure with a number of isochronous island between $m_1$ and $m_2$ that exist for a certain range of parameters. The bifurcation diagrams and the respective phase spaces are shown in Fig. 4.

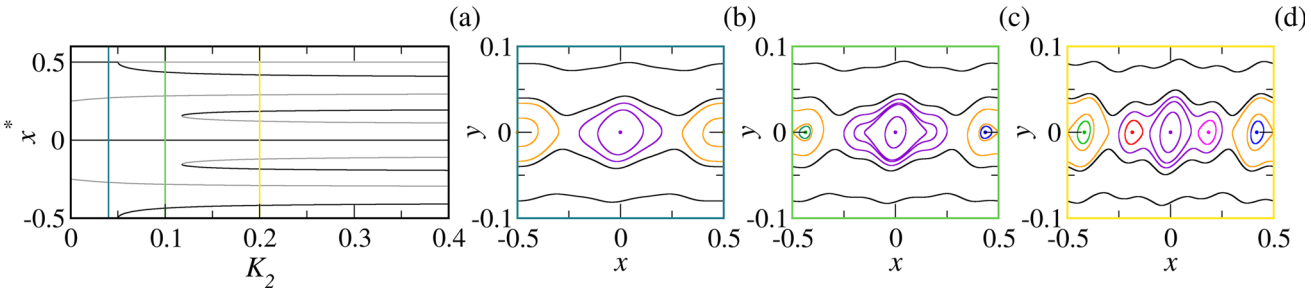


**Fig. 4** Transition with intermediate modes, for $m_1 = 2$, $m_2 = 5$ and $K_1 = 0.05$. The bifurcation diagram in panel (**a**) shows the evolution of the fixed points in the systems, where we observe first a pitchfork bifurcation followed by two saddle-node bifurcations. For the first mode, we have the phase space shown in (**b**) with $K_2 = 0.04$. The intermediate mode is represented in (**c**) for $K_2 = 0.1$. Finally, we have the predominance of the second mode in (**d**), where $K_2 = 0.2$. As in the previous figures, the colored dots represent elliptic points

In the bifurcation diagram of Fig. 4a, we observe two isochronous bifurcations occurring at different values of $K_2$. First, there is a pitchfork bifurcation in $K_2 = K_1 = 0.5$, where the elliptic point at $x = 0.5$ becomes hyperbolic and two new elliptic points emerge in the system. As a result, an intermediate mode arises, where three islands are present in the phase space. Second, we observe two saddle-node bifurcations at $K_2 \approx 0.13$, where two fixed points emerge around the elliptic point at $x = 0$. These two saddle-node bifurcations complete the $2 \to 5$ transition.

Just as in the case of Ref. [10], we analyze all the $m_1 \to m_2$ transitions with $m_1 \in [1, 5]$ and $m_2 \in [m_1 + 1, 6]$. All the bifurcation diagrams can be checked in the Supplementary Material [24].

## 4 Conclusions

The emergence of isochronous islands occurs due to the superposition of distinct resonant modes interacting on the same winding number surface. In the two-harmonic standard map, the integers $m_1$ and $m_2$ correspond to the two resonant modes acting on the system. Depending on the amplitudes $K_1$ and $K_2$, the system can exhibit between $m_1$ and $m_2$ islands, where $m_2 > m_1$.

We observed the emergence of new islands as the amplitude of the second mode increases, forming three types of isochronous transitions. The first one occurs through saddle-node bifurcations, where $(m_2 - m_1)$ pairs of elliptic and hyperbolic points emerge in the phase space for the same values of the parameters $K_1$ and $K_2$. Since we have the creation of fixed points, the saddle-node bifurcations are always supercritical.

The second route, from $m_1$ to $m_2$ islands, involves pitchfork bifurcations, where stable and unstable fixed points change their stability and two other fixed points with opposite stability emerge in the phase space. Finally, we have the isochronous transition with intermediate mode, i.e., the $m_1 \to m_2$ transition does not occur directly. For this last transition, we observe a combination of pitchfork and saddle-node bifurcations. In the diagram presented here, the pitchfork bifurcation occurs first, followed by simultaneous saddle-node bifurcations.

**Supplementary Information** The online version contains supplementary material available at https://doi.org/10.1140/epjs/s11734-025-01867-7.

**Acknowledgements** This research received the support of the Coordination for the Improvement of Higher Education Personnel (CAPES) under Grant No. 88881.895032/2023-01, the National Council for Scientific and Technological Development (CNPq - Grant No. 302665/2017-0, 403120/2021-7, 301019/2019-3, 443575/2024-0, 200428/2025-0), Fundação de Amparo à Pesquisa do Estado de São Paulo (FAPESP) under Grant No. 2024/03570-7 and 2024/05700-5 and CNEN (Comissão Nacional de Energia Nuclear) under Grant No. 01341.001299/2021-54.

**Data availability** The source code and data are openly available online in the Oscillations Control Group Data Repository [25].

## Appendix: Eigenvalue analysis for bifurcation identification

In discrete-time Hamiltonian systems, a periodic orbit is created, destroyed, or collides with another periodic orbit of the same period if the tangent map has an eigenvalue equal to unity, i.e., $\lambda = 1$ [26]. The process of creation, destruction or collision is a bifurcation process and it happens on a fixed point for a specific parameter value.

In terms of the eigenvalues of the tangent map, an elliptic point has complex eigenvalues that lie on the unit circle. In other hand, hyperbolic points have real eigenvalues and, for the two dimensional case, $|\lambda_1| > 1 > |\lambda_2|$ [22].

With the information presented above, we revisit the bifurcation diagram of Figs. 2, 3 and 4, and analyze the behavior of the eigenvalues on the bifurcation points. We compute the modulus of the two eigenvalues and analyze their imaginary parts. For elliptic points, the imaginary parts of the eigenvalues have the same magnitude but opposite signs, so we consider only the modulus of the imaginary part

In Fig. 2, we observe the emergence of a hyperbolic point along with an elliptic point after the bifurcation point, characterizing a saddle-node bifurcation. Following the eigenvalues for one bifurcation (all four bifurcation behave the same) we have the results presented in Fig. 5.

With the results presented in Fig. 5 , we identify a hyperbolic point in the lower branch of the diagram. For this branch, we observe two real eigenvalues with $|\lambda_1| > 1 > |\lambda_2|$ (first and second panels) and $\mathrm{Im}(\lambda) = 0$. For the upper branch, we have an elliptic point with modulus equal to one and non-null imaginary part. This result corroborates the observation from the diagram in Fig. 2, where we identify the emergence of elliptic and hyperbolic points after the bifurcation point, characterizing a saddle-node bifurcation.

Next, we analyze the pitchfork bifurcation presented in the diagram of Fig. 3. In a pitchfork bifurcation, one fixed point changes its stability, and two new fixed points—with the original stability of the initial fixed point—emerge in the phase space. The results for the pitchfork bifurcations are shown in Fig. 6.

Analyzing all the panels presented in Fig. 6, we observe a hyperbolic point, with zero imaginary part and eigenvalues satisfying $|\lambda_1| > 1 > |\lambda_2|$, changing its stability and becoming an elliptic point with complex eigenvalues

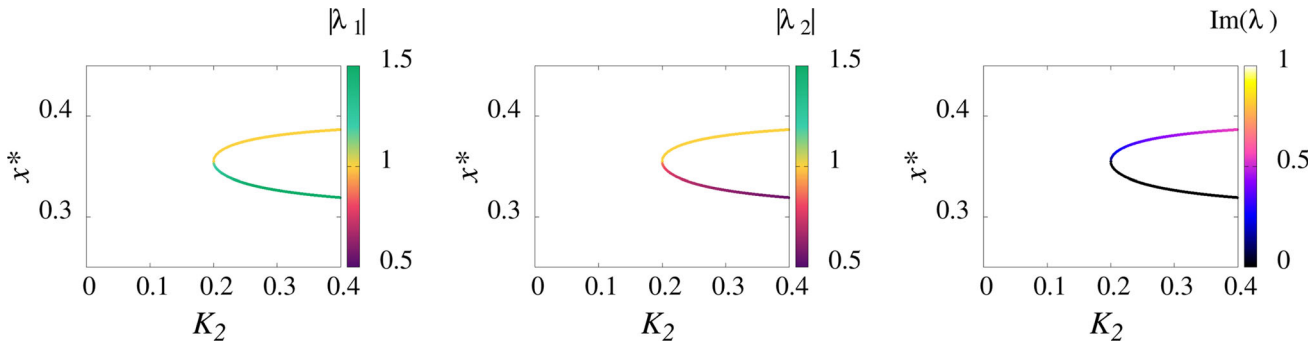


**Fig. 5** Eigenvalues for a saddle-node bifurcation presented in Fig. 2. For the first and second diagrams, red (green) points indicate modulus smaller (greater) than one, while yellow points indicate modulus equal to one. In the third panel we present the modulus of the imaginary part of the eigenvalues. In this case, black points indicate null imaginary part and colored points indicate non-null values

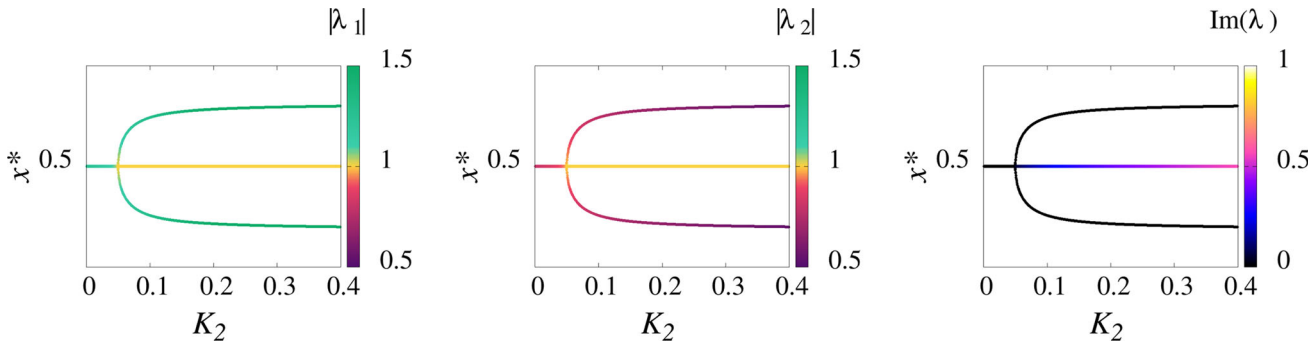


**Fig. 6** Eigenvalues for the pitchfork bifurcation presented in the diagram of Fig. 3. We use the same color scale of Fig. 5. In this bifurcation, we observe a hyperbolic point becoming an elliptic point, with two new hyperbolic points emerging on either side

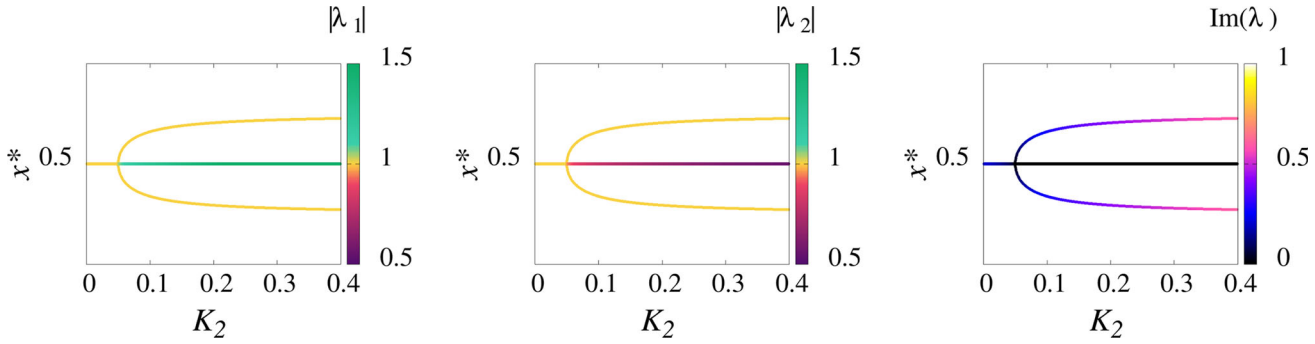


**Fig. 7** Eigenvalue analysis for the pitchfork bifurcation of Fig. 4. From the modulus analysis (first and second panel) and the information about the imaginary part (third panel), we conclude that an elliptic point changes its stability and two new elliptic points emerge in the system

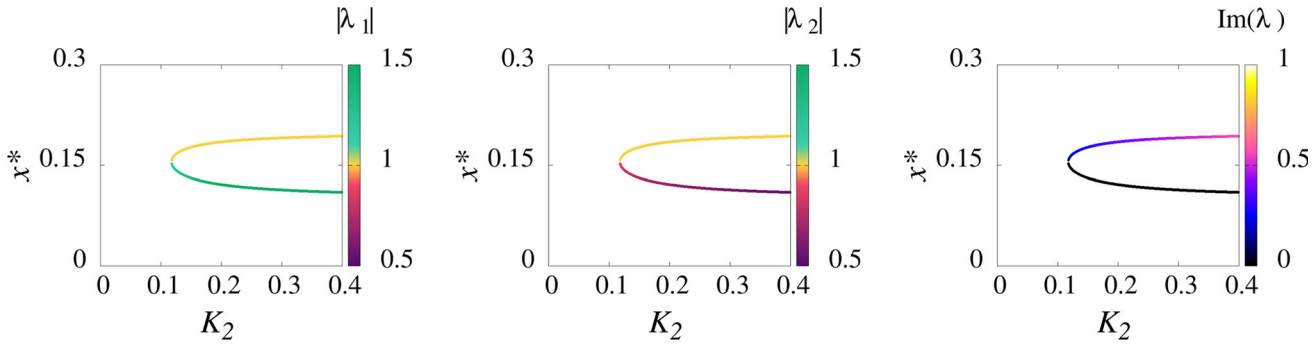


**Fig. 8** Configuration of the eigenvalues for a saddle-node bifurcation of the diagram in Fig. 4. We observe the emergence of a hyperbolic point (real values of $\lambda$) and a elliptic point (complex $\lambda$ with modulus equal to one) after the bifurcation point

and $|\lambda_{1,2}|= 1$. Along with this stability change, two hyperbolic points emerge on either side of the new elliptic point, characterizing a pitchfork bifurcation.

In the diagram of Fig. 4, we have both types of bifurcations as $K_2$ increases. The behavior of the eigenvalues are the same presented in Figs. 5 and 6. In Fig. 7, we present the eigenvalues associated with the pitchfork bifurcation shown in the diagram of Fig. 4. In this case, we observe an elliptic point changing its stability and becoming hyperbolic, with two new elliptic points emerging in the diagram. For the saddle-node bifurcations, we present the eigenvalues for one bifurcation in Fig. 8. Again, from the eigenvalue analysis, we observe the emergence of hyperbolic and elliptic points after the bifurcation point.

## References

1. L. Bardóczi, T.E. Evans, Experimental observation of magnetic island heteroclinic bifurcation in tokamaks. Phys. Rev. Lett. **126**(8), 085003 (2021)
2. T. Evans, W. Wu, G.P. Canal, N. Ferraro, Observations of heteroclinic bifurcations in resistive magnetohydrodynamic simulations of the plasma response to resonant magnetic perturbations. Phys. Rev. E **103**(1), 013209 (2021)
3. G.H. Walker, J. Ford, Amplitude instability and ergodic behavior for conservative nonlinear oscillator systems. Phys. Rev. **188**(1), 416 (1969)
4. M.C. Sousa, I.L. Caldas, A.M. Almeida, F.B. Rizzato, R. Pakter, Alternate islands of multiple isochronous chains in wave-particle interactions. Phys. Rev. E **88**(6), 064901 (2013)
5. M.J. Lazarotto, I.L. Caldas, Y. Elskens, Diffusion transitions in a 2d periodic lattice. Commun. Nonlinear Sci. Numer. Simul. **112**, 106525 (2022)
6. R.E. De Carvalho, A.O. De Almeida, Integrable approximation to the overlap of resonances. Phys. Lett. A **162**(6), 457–463 (1992)
7. J.D. Hermes, M. Hansen, S.S. Muni, E.D. Leonel, I.L. Caldas, Analysis of invariant spanning curves in oval billiards: A numerical approach based on slater's theorem. Chaos: An Interdisciplinary Journal of Nonlinear Science **35**(3), (2025)

8. B.B. Leal, I.L. Caldas, M.C. Sousa, R.L. Viana, A.M. Almeida, Isochronous island bifurcations driven by resonant magnetic perturbations in tokamaks. Phys. Rev. E **109**, 014230 (2024)
9. J. Fraile, C. André, M. Roberto, G.P. Canal, I.L. Caldas, Isochronous bifurcations of magnetic islands in tokamaks. Phys. Plasmas **31**(7), 072502 (2024)
10. M. Mugnaine, B.B. Leal, I.L. Caldas, A.M.O. Almeida, R.L. Viana, Isochronous bifurcations in a two-parameter twist map. Phys. Rev. E **110**(2), 024206 (2024)
11. A.J. Lichtenberg, M.A. Lieberman, *Regular and Chaotic Dynamics*, vol. 38 (Springer, New York, 2013)
12. B. Hasselblatt, A. Katok, *A First Course in Dynamics: with a Panorama of Recent Developments* (Cambridge University Press, Cambridge, 2003)
13. J.A. Ketoja, R.S. MacKay, Fractal boundary for the existence of invariant circles for area-preserving maps: observations and renormalisation explanation. Phys. D **35**(3), 318–334 (1989)
14. I. Satija, B. Sundaram, Interplay between symmetry breaking and quasiperiodicity in spin chains. Il Nuovo Cimento D **18**, 855–863 (1996)
15. H.E. Lomelí, R. Calleja, Heteroclinic bifurcations and chaotic transport in the two-harmonic standard map. Chaos: An Interdisciplinary Journal of Nonlinear Science **16**(2), (2006)
16. J.M. Greene, J.-M. Mao, Higher-order fixed points of the renormalisation operator for invariant circles. Nonlinearity **3**(1), 69 (1990)
17. J.M. Greene, H. Johannesson, B. Schaub, H. Suhl, Scaling anomaly at the critical transition of an incommensurate structure. Phys. Rev. A **36**(12), 5858 (1987)
18. J.A. Ketoja, Breakup of kolmogorov-arnol'd-moser tori of arbitrary frequency in a two-parameter system. Phys. Rev. A **42**(2), 775 (1990)
19. H. Johannesson, B. Schaub, H. Suhl, Critical exponents for an incommensurate structure with several length scales. Phys. Rev. B **37**(16), 9625 (1988)
20. R.C. Black, I.I. Satija, Universal pattern underlying the recurrence of kolmogorov-arnol'd-moser tori. Phys. Rev. Lett. **65**(1), 1 (1990)
21. E. Simonnet, H.A. Dijkstra, M. Ghil, Bifurcation analysis of ocean, atmosphere, and climate models. In: Handbook of Numerical Analysis vol. 14, pp. 187–229. Elsevier, Amsterdam (2009)
22. K.T. Alligood, T. Sauer, J.A. Yorke, *Chaos: an Introduction to Dynamical Systems* (Springer, New York, 2000)
23. J. Guckenheimer, P. Holmes, *Nonlinear Oscillations, Dynamical Systems, and Bifurcations of Vector Fields*, vol. 42 (Springer, New York, 2013)
24. See Supplemental Material at url for bifurcation diagrams of the fixed points for the combinations of $m_1 \in [1, 5]$ and $m_2 \in [m_1 + 1, 6]$
25. http://henon.if.usp.br/OscilControlData/IsochronousBifurcations/
26. L.E. Reichl, *Transition to Chaos* (Springer, New York, 2021)